USING gprMAX TO MODEL GROUND-PENETRATING RADAR (GPR) TO LOCATE CORN SEED AS AN ATTEMPT TO MEASURE PLANTING DEPTH

K. O. M. Mapoka, S. J. Birrell, M. Z. Tekeste, B. Steward, D. Eisenmann

ABSTRACT. *Planting depth (PD) plays an essential role in crop production by substantially impacting germination rates and yield potential. However, techniques to measure PD nondestructively have not been developed. A two-dimensional gprMax simulation study was conducted to investigate the effects of soil electromagnetic properties on ground-penetrating radar (GPR) waves. The primary objective was to examine the possibility of using GPR as a nondestructive sensor to detect subsurface corn seeds with the goal of measuring PD. A conventional fixed-offset gprMax antenna in contact with the soil surface was used in the simulations. Corn seed models of different materials and sizes were simulated, with properties of natural and synthetic (metal) corn seeds. The seed models were spherical, with radial dimensions of 0.006 and 0.024 m to simulate small and large corn seeds, respectively. Corn seed models were embedded in three homogeneous soil models (sandy loam, loam, and clay), and 1.6 and 2.6 GHz antenna models were used as excitation frequencies. A-scans and B-scans were obtained from the simulations. The A-scans showed that all targets (small natural corn and metal corn models, and large natural corm and metal corn models) successfully provided response amplitudes proportional to their dielectric properties in sandy loam and loam, but not in clay. In high bulk density soils, GPR waves failed to penetrate the soil models, and the targets were not detected. The 2.6 GHz antenna provided better response amplitudes from the targets. In the driest soil models (2.5%, and 5%), no response amplitude signatures were observed. In dry and relatively dry soil models (15%), the simulation times were much shorter to obtain a response amplitude from the targets (with feeble response amplitudes) compared to relatively wetter soils. To validate these models, laboratory experiments were conducted with three treatment factors (soil type, planting depth, and moisture content). In dry soils, corn seeds could be detected using a 2.6 GHz GPR antenna; however, the detection varied substantially within replicates of the same moisture group. Further research is necessary to understand the effects of soil moisture on the detection variability of buried corn seeds.*

Keywords. *Corn seed, Dielectric permittivity, Electromagnetic waves, Finite difference time domain, GPR, gprMax.*

Planting depth (PD) plays an essential role in crop production by substantially impacting germination rate and yield potential (Nielsen, 2001; Elmore et al., 2014; René-Laforest et al., 2014; Zhang et al., 2015). Significant research has been directed toward developing techniques that can control the downforce pressure on planter press wheels, as a strategy for maintaining a consistent PD over a given field topography, and control compaction by the planter depth control wheels. The control systems include hydraulic, mechanical, or pneumatic actuators. However, in many cases, the technologies fall short of the desired outcome, leading to uneven seedling emergence because of inconsistent PD due to incorrect setting of the downforce pressure for the field conditions. Several studies have shown the consequences of incorrect PD and the subsequent effects on germination and final yield (Hussen et al., 2013; Beck's Hybrids, 2014; Doerge et al., 2015). In their findings, Beck's Hybrids (2014) reported yield losses of 20% to 30%, and Doerge et al. (2015) reported yield losses of 5% to 9%. Due to the importance of PD on final yield, technologies to measure in-field PD during planting operations could have significant economic benefits. This study evaluated the potential of using ground-penetrating radar (GPR) as a nondestructive technique to measure seed PD in a closed trench.

GPR is a nondestructive geophysical technique that operates by transmitting and receiving electromagnetic waves reflected from features within a test material. It exploits the dielectric properties of the test material to map discontinuities and can furnish depth profiles of features in the test material. GPR can also provide high-resolution imagery of subsurface features, as governed by the antenna center frequency and the dielectric contrast of the test material. GPR technology has been applied broadly in agriculture; it has been used successfully to classify soil horizons and to locate buried roots and agricultural drainage pipes (Yoder et al., 2001; Odhiambo et al., 2002; Allred et al., 2004, 2005).

Submitted for review in February 2018 as manuscript number ITSC 12809; approved for publication as a Research Article by the Information Technology, Sensors, & Control Systems Community of ASABE in March 2019.

The authors are **Kenneth O. M. Mapoka,** Graduate Student, **Stuart J. Birrell,** Professor, **Mehari Z. Tekeste,** Assistant Professor, **Brian Steward,** Professor, and **David Eisenmann,** Adjunct Professor, Department of Agricultural and Biosystems Engineering, Iowa State University, Ames, Iowa. **Corresponding author:** Kenneth O. M. Mapoka, 2326 Elings Hall, Iowa State University, Ames IA 50011; phone: 515-708-7954; e-mail: komapoka@iastate.edu.

  ISSN 2151-0032 https://doi.org/10.13031/trans.12809

SOIL MIXING MODEL

Soils are inherently complex, and the effects of soil physical properties on GPR performance must be considered. GPR sensors respond to changes in dielectric properties. Soil physical properties that have potential to influence soil dielectric properties are the bulk density, composition (sand, silt, and clay content), moisture content, and particle density. Thus, soil mixing models have been developed to predict the influence of soil physical properties on soil dielectric properties (Peplinski et al., 1995). A soil mixing model is a semi-empirical dielectric model that estimates the real and imaginary components of the dielectric permittivity (dispersive material properties) of a soil. Soil mixing models have been used to relate soil physical properties and soil composition with the dielectric permittivity and electrical conductivity of bulk soil (Miller et al., 2004; Chen et al., 2014). A realistic soil model can be modeled based on stochastic distributions of the soil properties. Some researchers have referred to these models as pedo-transfer functions in which soil dielectric properties are functions of the natural soil composition (Hendrickx et al., 2003).

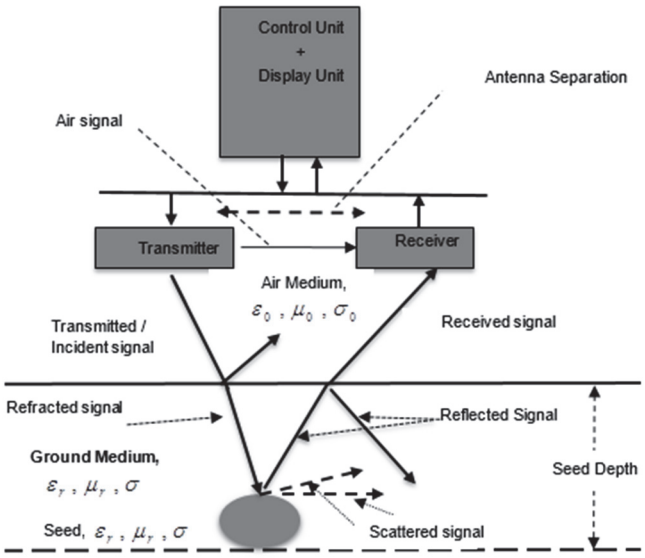

Figure 1. GPR operating principles showing the antenna separation and the transmitted, refracted, and reflected waves from the air-soil and soil-seed interfaces (Sato, 2009).

GPR OPERATION PRINCIPLES

A typical GPR system consists of a transmitter antenna and a receiver antenna. The two antennas may be separated by some distance or packaged as a combined transmitter/receiver antenna. The antennas are located above the soil surface at a height determined by the operator. GPR transmits electromagnetic waves into the soil at center frequencies that can range from ~100 Hz to 2.6 GHz. In most cases, the center frequency is associated with the application and desired resolution. Electromagnetic waves are transmitted into the test material, and depending on the material's dielectric properties, some fraction of the energy is reflected, while the remaining energy is transmitted through the material or absorbed by the material. Additionally, the center frequency and the dielectric properties of the test material can lead to polarization of the material, which can affect wave propagation (Neal, 2004; Sadiku, 2010). A typical GPR system includes a common-offset bistatic antenna placed near the soil surface, transmitting waves into the soil and receiving reflected waves from both the air-soil and soil-seed interfaces, as governed by the dielectric properties of each material (fig. 1). In GPR terminology, a plot of the reflected wave amplitude as a function of time is called a trace or A-scan. The A-scan represents a single static response from a target (fig. 4). Moving the GPR antenna along a flat soil surface while collecting and recording data at different spatial positions results in a B-scan. The B-scan is made up of a series of A-scans merged for a given spatial distance, represented as a two-dimensional image (2-D) with time of flight on the *y*-axis and spatial distance on the *x*-axis.

ELECTROMAGNETIC THEORY

Electromagnetic (EM) theory involves the study of moving EM fields in a given space and time. EM theory is governed by Maxwell's equations and constitutive laws (Jol, 2009; Sadiku, 2010). The constitutive laws define the dielectric properties that govern the behavior of EM signals moving through a test material. The constitutive laws employ three dielectric properties: electrical conductivity (σ), dielectric permittivity (ε), and magnetic permeability (μ). These dielectric properties describe a material's relationship with the EM field (Norimoto, 1976; Odhiambo et al., 2002; Orfanidis, 2002; Neal, 2004; Annan, 2009; Jol, 2009; Sadiku, 2010). In this study, the dielectric properties of soils were estimated using soil mixing models, and the subsequent effects on EM wave propagation were modeled. EM wave technology has been used in numerous agricultural sensing applications (Topp et al., 1980; Brisco et al., 1992; Yoder et al., 2001; Odhiambo et al., 2002; Allred et al., 2004, 2005, 2008). This study examined the possibility of determining corn seed depth using EM waves, which has not been previously investigated.

gprMAX MODELING

An open-source GPR modeling package called gprMax (GNU General Public License v3) was developed to simulate GPR wave propagation for diverse applications by simulating the responses from different target materials and sizes (Warren et al., 2016). This software solves Maxwell's equations in 2-D or 3-D by employing the finite difference and time domain (FDTD) numerical method. FDTD is a numerical analysis method for modeling computational electrodynamics (Yee, 1966) by solving partial differential equations to estimate the spatial description of electric and magnetic fields. FDTD discretizes Maxwell's functions in space and time by using the central differences method. Two parameters, cell size (Δx, Δy, Δz) and time step (Δt), are used to discretize the domain with specific spatial and temporal resolutions, which affect the FDTD accuracy. The cell size needs to be smaller than the smallest wavelength. In modeling GPR wave propagation, the cell size has to be at least one-tenth less than the propagating electromagnetic wavelength (i.e., $\Delta x = \lambda/10$) to minimize numerical errors within an orthogonal grid. In this study, this criterion was used for selecting the most effective cell size and time step. The time step must

be less than the ratio of the cell size and the speed of light (c, m s^{-1}) to satisfy the Courant limit condition that relates the stability of the spatial discretization to the required time step. The discretized components follow the Yee cell lattice, in which the constitutive properties for a particular medium are defined per cell joint of the Yee cell (Kunz and Luebbers, 1993; Ketata et al., 2010; Schneider, 2010; Warnick, 2011).

The FDTD framework uses the Yee scheme, in which the two complementary meshes of the electric and magnetic fields components are solved alternately. Yee (1966) termed the principle "leapfrog," as the electrical component at time t is used to calculate the magnetic component at time $+0.5\Delta t$ and, in turn, the electrical component at time ($t + \Delta t$). The sequential updating of the two components continues until the defined simulation time (time window) has elapsed. The absorbing boundary conditions are defined to truncate an infinite simulation domain to a finite size. Fields reaching the edge of the medium are truncated and absorbed, preventing reflections into the computational domain; hence, all components are zero at the boundaries. In this study, a Gaussian waveform signal source was defined and injected into the gprMax model to initiate wave propagation (Warren et al., 2016).

This study investigated the possible use of GPR for detecting corn seeds in a closed furrow with different soil conditions. The objectives of this study were to:

1. Model GPR transmission through a lossy medium.
2. Evaluate the probability of using GPR to detect corn seeds in a closed furrow with different soil conditions.
3. Investigate the effects of corn seed material and size on corn seed response.

METHODOLOGY

SEED MODEL PROPERTIES

In the simulation model, two materials were modeled to represent corn seeds with two different sizes. First, the physical and dielectric properties of corn (*Zea mays*) seeds were used. Second, a synthetic seed was modeled using the conductance of metal. These two seed models helped us to develop an understanding of the effects of seed material and size on the energy reflected from the seeds. Corn seeds have distinct shapes that can be modeled using conical, rectangular, triangular, or even spherical forms (fig. 2a). In the model, a spherical shape was used because it represented corn seeds well and was easy to implement. Measurements to estimate seed size were taken from a sample of 50 corn kernels. A digital caliper with 0.01 mm resolution was used to acquire these measurements (fig. 2b). The rectangular length, width, and thickness of each kernel were measured and averaged to estimate the mean kernel size and rectangular volume of the sample corn harvested in 2016 (20% MC, Iowa State University farm, Boone County, Iowa). The equivalent spherical volume was determined, and the corresponding spherical radius was 0.006 m. Thus, a spherical corn seed model was implemented with a 0.006 m radius and classified as a small size kernel. To evaluate the effect of kernel size, a large spherical corn kernel model was implemented with a radius four times that of the small kernel model (i.e., 0.024 m).

Research by Nelson (1987, 2005) and Trabelsi and Nelson (2003) predicting the dielectric permittivity of bulk corn samples enabled estimation of the dielectric permittivity of a single corn kernel. The bulk dielectric permittivity of corn is a function of the bulk density, single-kernel density, moisture content, temperature, and frequency. The bulk density of corn is 0.7208 g cm^{-3} (56 lb bu^{-1}); for a single kernel, the density ranges from 1.27 to 1.38 g cm^{-3} (Mészáros, 2007). The optimum moisture content is 11% for corn kernels stored at room temperature of 12.78°C to ensure the highest possible percentage germination rate (Sayre, 1940). Therefore, the dielectric permittivity of a single kernel was calculated according to the models developed by Nelson and Datta (2001) and Nelson (2015) for corn kernels with 11% moisture content, 1.275 g cm^{-3} kernel density, and 0.7208 g cm^{-3} corn bulk density.

The relative dielectric permittivity (ε_r) of a single corn

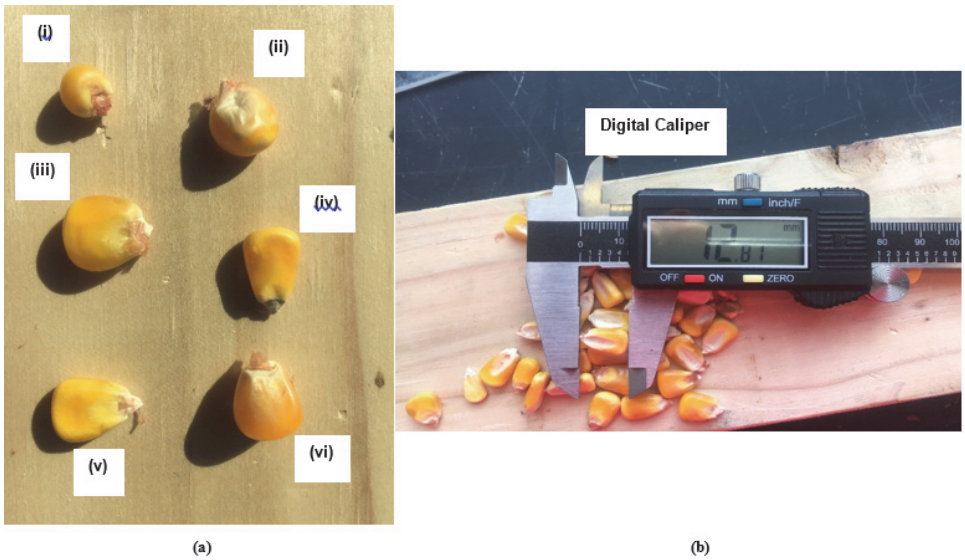

Figure 2. (a) Images of corn shapes, including circular/roundish/sphere shapes (i, ii, vi) and triangular/conical shapes (iii, iv, v), and (b) measurement of corn dimensions using a digital caliper.

seed was estimated to be 3.90 (unitless), and the magnetic permeability (μ_r) of a dielectric or food material is usually equal to the permeability of free space: $\mu_0 = 4\pi \times 10^{-7}$ H m^{-1} (Datta, 2001). Therefore, the relative magnetic permeability (μ_r) of the corn seed models was set to 1 (unitless). Corn seeds in storage have low moisture levels; therefore, they have extremely low ionic movement, which leads to low ionic conductivity. However, based on Datta (2001), the electrical conductivity (σ, S m^{-1}) of a dielectric or food material is directly related to the dielectric permittivity and frequency (f, Hz), given as $\sigma = \omega\varepsilon$, where ω is the angular frequency ($\omega = 2\pi f$ rad s^{-1}), and ε is the dielectric permittivity (F m^{-1}). Metals (e.g., stainless steel) are highly conductive or perfect electrical conductors (PEC). PEC is a built-in material function in gprMax (Warren et al., 2016). Based on the electrical conductivity table for metals, a stainless steel corn seed was defined to have an electrical conductivity of $\sigma = 1.45 \times 10^6$ S m^{-1} (ECT, 2013). The electrical conductivity of a metal overshadows its dielectric permittivity polarization effect; therefore, the relative dielectric permittivity and permeability of stainless steel were defined as $\varepsilon = -1$ (unitless) and $\mu = 1$ (unitless) (Howlader and Sattar, 2015).

Soil Model Properties

Soil heterogeneity is known to adversely affect GPR performance by decreasing the signal-to-noise ratio due to dielectric discontinuities in the soil, which leads to additional reflections or random scattering back to the soil surface, consequently masking the intended target responses. For instance, Chaudhari (2015) found that the organic matter content in a soil had a substantial impact on the soil's dielectric properties. An increase in the soil organic matter content increased both the soil dielectric permittivity and loss factor. The soil surface roughness due to soil irregularities (e.g., rocks, soil texture, aggregates) can also have an impact on incidental waves and polarization, which may affect wave penetration (Flores et al., 2009). For instance, on rough surfaces, it is possible to have step changes in the dielectric properties of heterogeneous soils, which can influence GPR wave propagation.

In general, waves are more diffuse on rough surfaces and more directional on flat surfaces, and rough soil surfaces may lead to total absorption of the transmitted wave by the dielectric medium, a phenomenon referred to as Brewster angle (Hajnsek and Papathanassiou, 2005). Therefore, in the proposed lossy soil models, the soil surface was considered flat, and other interferences that could cause unwarranted backscatter, such as grass and woody materials (organic matter) were not included to reduce model complexity. In the developed models, the soil was assumed to be homogeneous, time-invariant, and isotropic. The homogeneity assumptions made the soil models linear, providing an explicit and easy understanding of the numerical results as influenced by critical soil and target factors that could limit *in situ* GPR wave surveys (Twizere, 2011). However, these model assumptions also suppressed *in situ* soil conditions that are likely to degrade GPR waves during actual GPR measurements to locate corn seeds.

Soil mixing models were used to predict the soil dielectric permittivity and electrical conductivity. Three soil physical properties were investigated: volumetric moisture content (VMC), soil composition (sand, silt, and clay content), and soil bulk density. Typically, the soil VMC at planting is 15.00% to 40.00% (Weiler et al., 1998), where 15.00% is the minimum soil moisture required at planting. Therefore, in our simulation, two VMC values (2.5% and 5%) below the minimum required soil moisture and three VMC values (15%, 25%, and 40%) within the acceptable soil moisture range were investigated.

Three soil textures were investigated: sandy loam, loam, and clay. The soil compositions for the three soil textures, shown in table 1, were based on the Soil Survey Laboratory Information Manual (NSSC, 2011). In addition, three soil bulk densities were assessed: two standard (acceptable) soil bulk densities at planting were used to compute soil dielectric properties: 1.42 g cm^{-3} for the sandy loam soil, and 1.2 g cm^{-3} for the loam and clay soils (Hillel, 2003). A third soil bulk density (3.00 g cm^{-3}) was selected for all soil textures to investigate the impact of high soil bulk density on GPR wave propagation. The selection of the bulk density values was based on the soil bulk density of <1.60 g cm^{-3} required at planting.

A soil particle density of 2.66 g cm^{-3} was used for all simulations (Hendrickx et al., 2003; Miller et al., 2004). Because soils are inherently heterogeneous, it is challenging to understand the individual effects of different soil parameters (e.g., VMC, bulk density, and soil composition) on sensor response. In the simulation, three soil textures (sandy loam, loam, and clay) were used with different soil conditions. For each soil texture, one soil property was varied at a time, while the other properties were kept constant. With this approach, a range of soil dielectric properties was determined as a function of the different soil properties (tables 2 and 3) to investigate the effects of individual soil properties.

Water has high relative dielectric permittivity (~81), which influences the effective soil dielectric permittivity. The soil texture (e.g., clay) and soil bulk density mainly influenced the soil electrical conductivity (tables 2 and 3). When the soil bulk density was increased to 3 g cm^{-3}, each soil had increased soil electrical conductivity. These soil electrical properties were used in gprMax to evaluate the possibility of using GPR to detect different target materials and sizes.

Model of a Seed in the Soil

A 2-D simulation model consisting of a homogeneous distribution of relevant soil properties and seed dielectric properties was developed and used as the input to the gprMax software. The 2-D model was used to investigate the likelihood of obtaining a response from embedded corn seeds within the soil model. The corn seed targets were modeled to be at a 0.07 m depth in the soil medium. The 2-D model specified a rectangular domain with dimensions of

Table 1. Soil compositions used to determine soil dielectric properties.

	Soil Composition		
Soil Texture	Sand	Silt	Clay
Sandy loam	60%	22%	18%
Loam	48%	30%	22%
Clay	20%	10%	70%

Table 2. Estimated dielectric permittivity and electrical conductivity of sandy loam, loam, and clay at different soil bulk densities.

Volumetric Moisture Content (VMC, %)	Sandy Loam at 1.42 g cm^{-3}		Loam at 1.2 g cm^{-3}		Clay at 1.2 g cm^{-3}	
	Permittivity	Conductivity (S m^{-1})	Permittivity	Conductivity (S m^{-1})	Permittivity	Conductivity (S m^{-1})
2.50	3.41	0.04	2.89	0.05	2.72	1.35
5.00	4.25	0.04	3.55	0.05	3.24	1.35
15.00	8.30	0.04	6.96	0.05	6.09	1.35
25.00	13.59	0.04	11.60	0.05	10.18	1.35
40.00	23.84	0.04	21.04	0.05	18.91	1.35

Table 3. Estimated dielectric permittivity and electrical conductivity of sandy loan, loam, and clay at soil bulk density of 3.00 g cm^{-3}.

Volumetric Moisture Content (VMC, %)	Sandy Loam		Loam		Clay	
	Permittivity	Conductivity (S m^{-1})	Permittivity	Conductivity (S m^{-1})	Permittivity	Conductivity (S m^{-1})
2.50	6.58	3.14	6.31	3.40	6.05	4.84
5.00	7.76	3.14	7.31	3.40	6.85	4.84
15.00	13.29	3.14	12.32	3.40	10.94	4.84
25.00	19.98	3.14	18.53	3.40	16.40	4.84
40.00	32.35	3.14	30.37	3.40	27.37	4.84

0.24, 0.21, and 0.002 m (x, y, z; 2-D models in gprMax are a single-cell slice of a 3-D model), whereby the soil model coordinates within the rectangular domain were at 0, 0, 0 m (bottom corner) and 0.24, 0.17, 0.002 m (top corner), creating a space for the antenna above the soil (fig. 3). The geometric model shown in figure 3b was stored as a *vti* object file, and a paraview package was used to display the geometry (a paraview package is a visualization tool used to display gprMax simulation images in *vti* format). The wave was discretized in space and time with a cell size of $\Delta x = \Delta y = \Delta z = 0.002$ m and a time step of $\Delta t = 4.717$ ps. This cell size was maintained throughout the simulation.

A lossy soil medium was defined by the dielectric permittivity, the magnetic permeability, and the soil electrical conductivity, as described in the Soil Model Properties section. The simulation time window was specified to be 5 ns. The algorithm was designed to have perfectly matched layer (PML) absorbing boundaries conditions (ABC), which enclosed the entire simulation domain at the edges. The purpose of the absorbing boundaries conditions was stated earlier in the gprMax Modeling section; further information on ABC is presented by Mur (1981, 1998) and Schneider (2010).

A Gaussian pulse waveform was provided as the excitation source in the gprMax model. The Gaussian waveform source had a current source of 1 A with a pulse time of 5.3125×10^{-8} s. The polarization was specified to be in the z-direction. The specified current was converted internally by the gprMax software to a related electric field strength amplitude in V m^{-1} (herein referred to as the response amplitude). Based on the dielectric properties specified in the simulation model, the response amplitudes were simulated (tables 4 through 6). Simulations were conducted at two frequencies: 1.6 and 2.6 GHz. A conventional fixed-offset antenna was used in the simulations, whereby the antenna was positioned directly on top of the soil surface and stepped at increments of 0.002 m across the x-direction (horizontal) of the domain to locate the buried seed target. Every time the antenna was moved, a new A-scan was recorded; therefore, 60 A-scans were specified to create the B-scan. The total horizontal distance covered by the transmitter and receiver as they moved over the corn seed model was 0.12 m. The A-scan results were exported to Matlab for visualization.

RESULTS AND DISCUSSION

In the GPR A-scans, the responses due to reflections at the air-soil and soil-seed interfaces can be observed (fig. 4). The response amplitudes for both target materials were reasonable and as expected. However, the responses at 2.5% and 5% VMC are not included in the plots because they had very low response amplitudes. Second reflections from the bottom of the large natural corn seed (0.024 m radius) were observed (fig. 4b). The small natural corn seed did not have observable second reflections (fig. 4a). The electric field interactions with the large seed provided higher peak response amplitudes compared to the small seed. The GPR wave response to the small seed approximated Raleigh scattering, as the natural corn seed model was small in comparison to the dominant pulse wavelength.

All A-scans showed a clear soil reflection (fig. 4). The magnitude of the signal transmitted into the soil decreased proportionally according to the magnitude of the soil dielectric permittivity and electrical conductivity. The dielectric contrast governed wave reflections at the air-soil and soil-seed interfaces; hence, the response amplitudes shown in figure 4 indicate the magnitude of the dielectric contrast between media in the model. For relatively dry soils, the reflections at the air-soil interface were lower, and the energy transmitted into the soil was higher, compared to wet soils.

In contrast, at higher soil VMC (25% and 40%), the soil absorbed a significant proportion of the GPR energy that was transmitted into the soil, and more energy was reflected at the air-soil interface. Higher VMC contributed to a higher dielectric contrast between the natural corn seed and the soil model, and hence the relatively higher response amplitudes in lossy wet soils (fig. 4). However, this phenomenon was the opposite for the metal seed models, for which the response amplitudes decreased with an increase in VMC (tables 4 and 5). In drier soils (≤15% VMC), the simulation time was much shorter for the response amplitude from corn seeds (i.e., less computation time was required to compute a model solution) compared to simulations with wetter soils.

As expected, the response amplitudes from wetter soils exhibited a longer time of flight (fig. 4), which means that the GPR wave velocity was reduced with high soil VMC. This phenomenon was observed for both the natural and

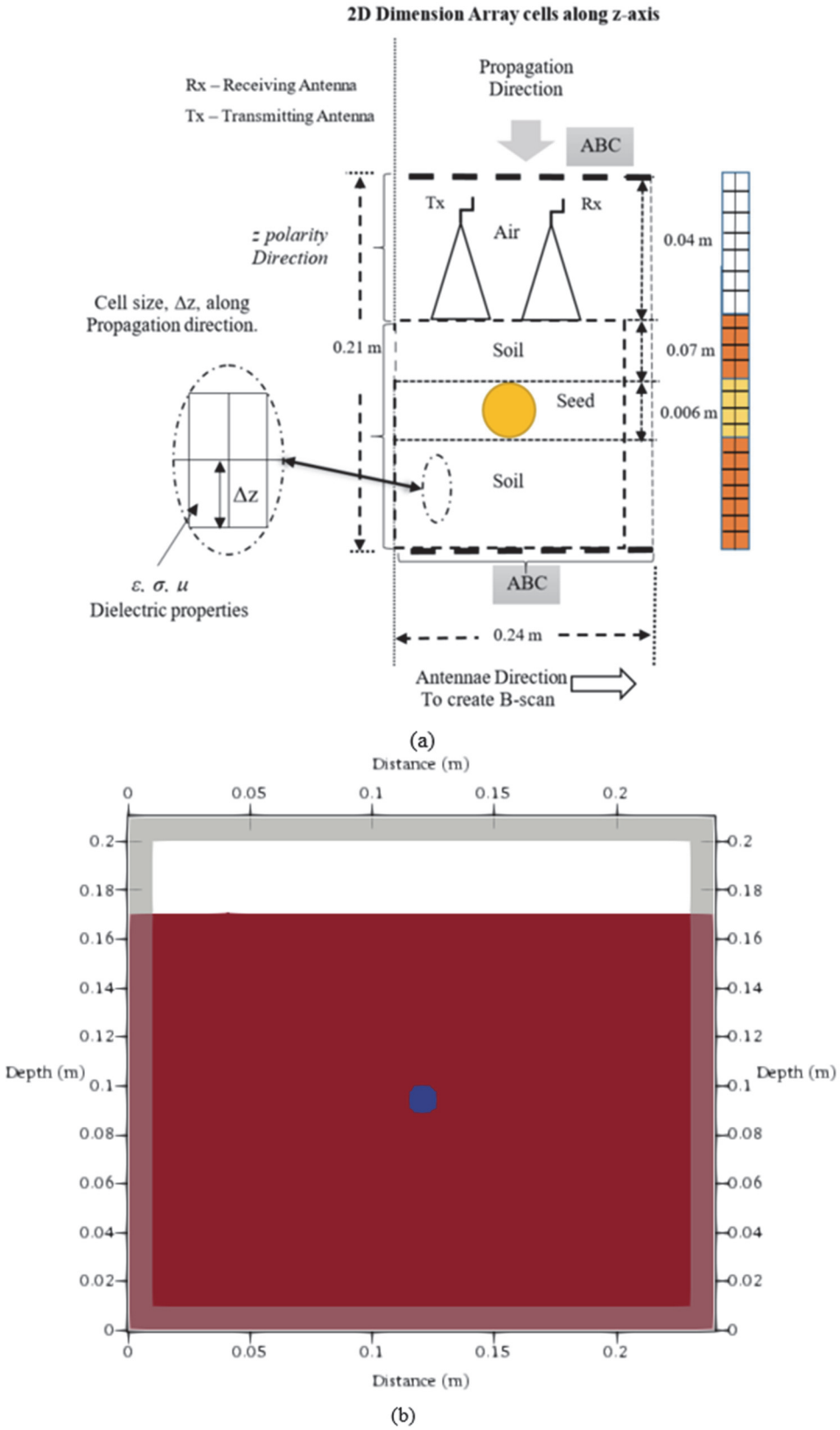

Figure 3. (a) 2-D model of a corn seed embedded 0.07 m deep in the soil with a pulsing antenna source directly on top of the soil surface (a small section is enlarged to show the cell size and dielectric properties that define each cell), and (b) gprMax geometrical model of a spherical seed embedded 0.07 m deep in the soil.

metal corn seed models. Throughout the simulations, the soil bulk density was kept constant for the sandy loam, loam, and clay soils, respectively.

The response amplitudes were extracted from the A-scans and recorded to indicate the presence of corn seed models. The magnitude of the response amplitude was proportional

Table 4. Simulation results for soil bulk density of 1.42 g cm^{-3} and different VMC in sandy loam using an antenna frequency of 1.6 GHz.

Volumetric Moisture Content (VMC, %)	Small Natural Corn Seed Model		Large Natural Corn Seed Model	
	Time of Flight (ns)	Peak Response Amplitude (V m^{-1})	Time of Flight (ns)	Peak Response Amplitude (V m^{-1})
2.50	2.00	16	1.61	36
5.00	2.02	21	1.80	38
15.00	2.09	53	2.15	80
25.00	2.50	64	2.54	119
40.00	3.00	74	3.04	167
Volumetric Moisture Content (VMC, %)	Small Metal Corn Seed Model		Large Metal Corn Seed Model	
	Time of Flight (ns)	Peak Response Amplitude (V m^{-1})	Time of Flight (ns)	Peak Response Amplitude (V m^{-1})
2.50	1.47	318	1.46	408
5.00	1.57	309	1.56	406
15.00	1.97	292	1.96	425
25.00	2.36	278	2.35	430
40.00	2.94	256	2.93	415

Table 5. Simulation results for soil bulk density of 1.2 g cm^{-3} and different VMC in loam using an antenna frequency of 1.6 GHz.

Volumetric Moisture Content (VMC, %)	Small Natural Corn Seed Model		Large Natural Corn Seed Model	
	Time of Flight (ns)	Peak Response Amplitude (V m^{-1})	Time of Flight (ns)	Peak Response Amplitude (V m^{-1})
2.50	1.71	39	1.67	32
5.00	1.80	44	1.70	28
15.00	1.98	46	2.03	63
25.00	2.36	55	2.41	98
40.00	2.95	68	2.99	154
Volumetric Moisture Content (VMC, %)	Small Metal Corn Seed Model		Large Metal Corn Seed Model	
	Time of Flight (ns)	Peak Response Amplitude (V m^{-1})	Time of Flight (ns)	Peak Response Amplitude (V m^{-1})
2.50	1.41	271	1.39	359
5.00	1.50	267	1.48	363
15.00	1.85	257	1.84	383
25.00	2.24	252	2.21	396
40.00	2.85	241	2.80	397

Table 6. Simulation results for natural corn seed models in sandy loam at soil bulk density of 1.42 g cm^{-3} using a frequency of 2.6 GHz.

Volumetric Moisture Content (VMC, %)	Small Natural Corn Seed Model		Large Natural Corn Seed Model	
	Time of Flight (ns)	Peak Response Amplitude (V m^{-1})	Time of Flight (ns)	Peak Response Amplitude (V m^{-1})
2.50	1.34	24	1.35	35
5.00	1.37	28	1.37	28
15.00	1.86	65	1.88	97
25.00	2.27	86	2.28	169
40.00	2.88	94	2.90	242

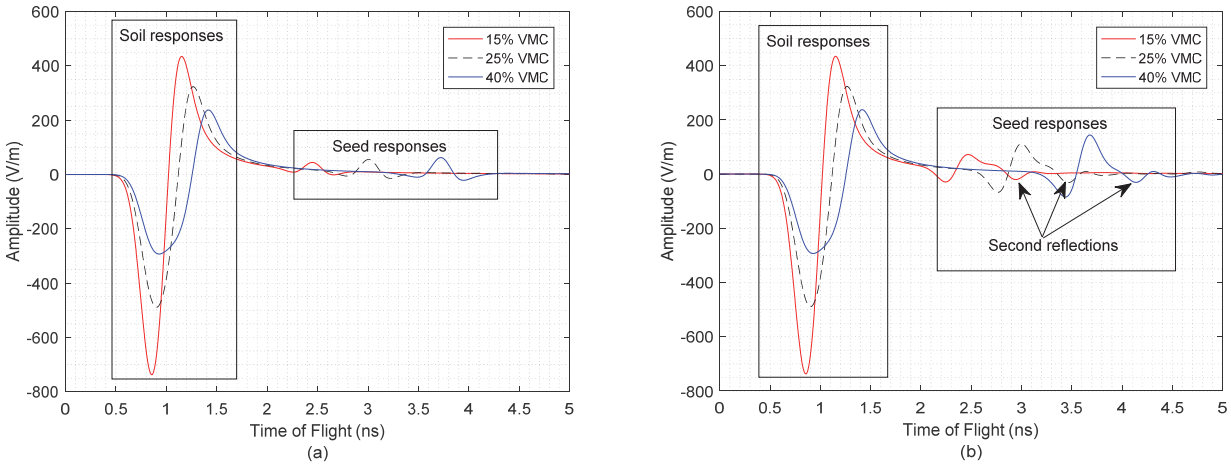

Figure 4. A-scans for evaluating transmission of GPR waves through sandy loam soil at different volumetric moisture contents (VMC) with (a) small natural corn seed model (0.006 m radius) and (b) large natural corn seed model (0.024 m radius).

to the dielectric properties causing the change at the soil-seed interface, the GPR wave frequency, and the size and material of the corn seed model. The time of flight was influenced by the soil conditions, which governed the transmission of GPR waves through the soil model (tables 4 through 6).

The metal seed models were subjected to the same soil simulation parameters used for the natural seed models, as listed in tables 2 and 3. The metal seeds were distinguishable by their response amplitudes, which were associated with size. The large metal seeds had higher response amplitudes compared to the small metal seeds (tables 4 and 5). The time of flight trends were similar to natural corn seeds when soil VMC was high. Large seeds provided a large surface area with which the GPR wave could interact. Regardless of size, metal corn seeds were highly responsive to GPR waves in dry and wet sand and loam soil conditions. At the driest soil conditions (2.5% VMC), the response amplitudes for both metal seed sizes were large. Unlike the natural corn seeds, the metal seeds did not have strong second reflections because metals are highly conductive. The electric field reaching the conductive seed induces a magnetic field that creates a current flow in the conductor, leading to a zero net electric field within the conductor. Thus, the entire GPR wave was reflected. Moreover, as the GPR wave traveled through wet soil, it was subjected to higher impedance due to the VMC and soil composition.

The clay soil had high electrical conductivity, which created high impedance and attenuation during GPR wave propagation. In the simulations, a small proportion of the transmitted wave penetrated the soil surface and instantly decayed to zero, failing to reach the corn seed targets. No response amplitude was registered from the embedded seed models in the clay soil. A higher proportion of the GPR wave was reflected at the soil interface. The model indicated that clay-rich soils might present challenges that would complicate GPR mapping of seeds. Neither target (natural or metal) provided a response amplitude in the clay soil.

Soil Bulk Density and Antenna Frequency

The effects of high soil bulk density (3 g cm^{-3}) and antenna frequency were evaluated. High soil bulk density adversely impacted GPR wave propagation by increasing the soil dielectric permittivity and electrical conductivity. These two parameters contributed to high soil impedance, creating an impenetrable and highly attenuating soil surface. As with the clay soil, high soil bulk density confounds GPR sensing applications. The high bulk density completely impeded GPR waves from entering the soil, making them unable to detect the target. Thus, no target response was observable in high bulk density soil. In addition, with the same high bulk density at the higher frequency of 2.6 GHz, shallowly embedded seed models could not be mapped due to high attenuation or absorption of the signal.

Consequently, there were no obvious target responses with high clay content and high soil bulk density at 2.6 GHz. However, when the high frequency was used with sandy loam soil with a low soil bulk density of 1.42 g cm^{-3}, all targets (small natural corn and metal corn, and large natural corn and metal corn) were observed with larger response amplitudes. Table 6 presents the responses from the small and large natural corn seed models in sandy loam.

The high center frequency (2.6 GHz) led to shorter wavelengths and increased resolution, which improved the response amplitudes of small and shallow corn seed models in the sandy loam and loam soils. For instance, at the low center frequency (1.6 GHz), the response amplitudes for small natural corn seeds (0.006 m radius) were low (fig. 4a and table 4). However, for similar sandy loam soil conditions at 2.6 GHz, the response amplitudes increased by approximately 25.00% compared to the response amplitudes shown in table 4. For the large natural corn seed, the increase was approximately 30.00%. For all targets, the higher frequency provided larger response amplitudes for both target sizes.

This simulation study evaluated soil conditions and targets that would lead to successful GPR detection and identified soil conditions in which seeds could be detected by GPR after planting. For instance, clay-rich and denser soils should be avoided because of rapid attenuation in those conditions. Conversely, a higher center frequency would be beneficial, as the high center frequency (2.6 GHz) provided higher response amplitudes than the low center frequency (1.6 GHz).

The B-scans shown in figures 5 through 8 illustrate the dielectric contrast between the modeled soil and seed. A

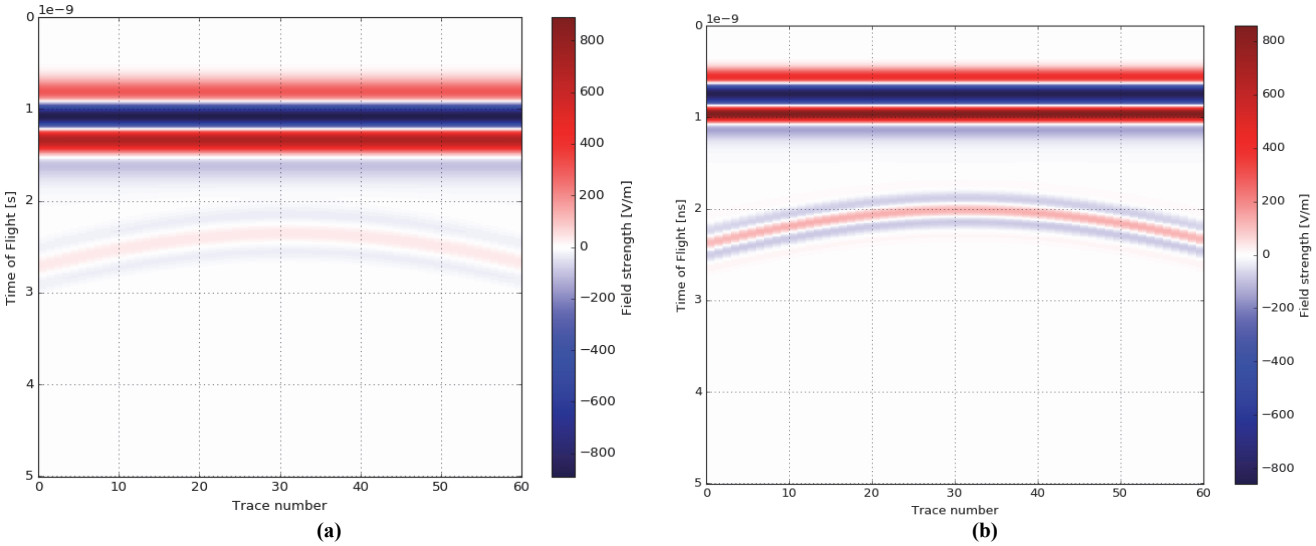

Figure 5. Response of small natural corn seed model (0.006 m radius) in sandy loam at 15% VMC and soil bulk density of 1.42 g cm^{-3}: (a) B-scan at center frequency of 1.6 GHz, and (b) B-scan at center frequency of 2.6 GHz.

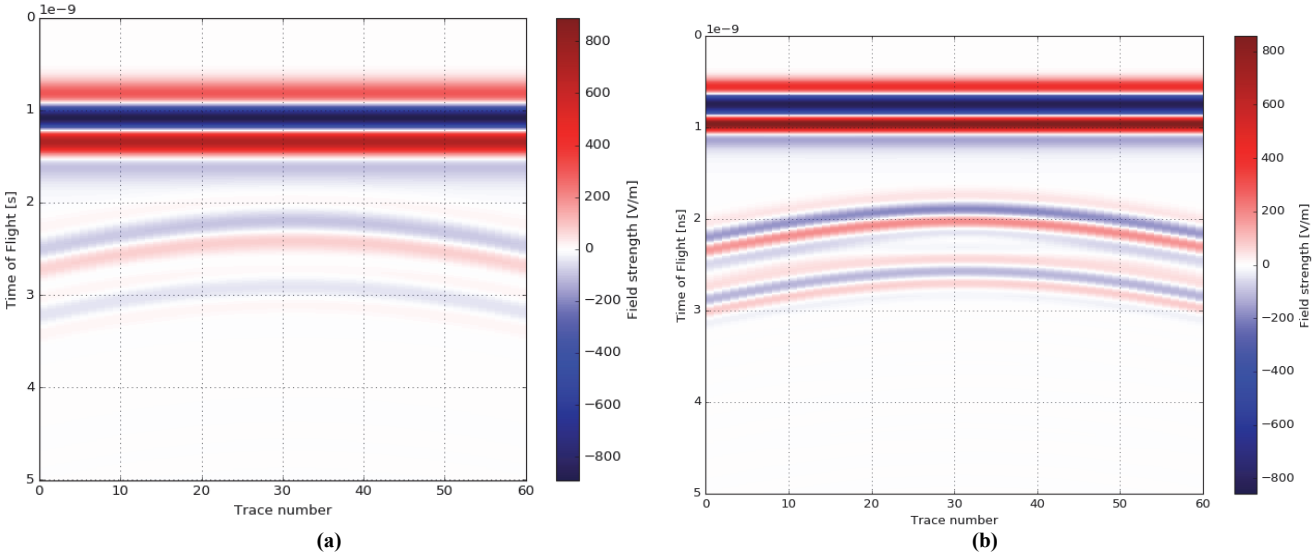

Figure 6. Response of large natural corn seed model (0.024 m radius) in sandy loam at 15% VMC and soil bulk density of 1.42 g cm^{-3}: (a) B-scan at center frequency of 1.6 GHz, and (b) B-scan at center frequency of 2.6 GHz.

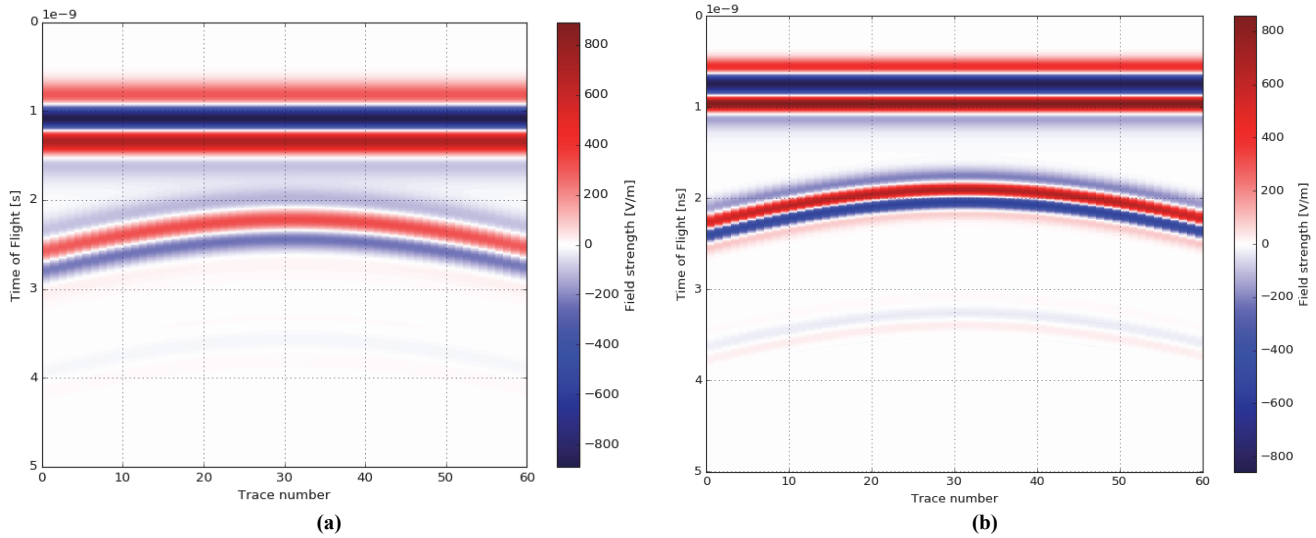

Figure 7. Response of small metal corn seed model (0.006 m radius) in sandy loam at 15% VMC and soil bulk density of 1.42 g cm^{-3}: (a) B-scan at center frequency of 1.6 GHz, and (b) B-scan at center frequency of 2.6 GHz.

stronger blue color in the B-scans indicates a higher negative response amplitude, and a brighter reddish color indicates a higher positive response amplitude. The implication is that a dielectric material (soil or seed) has a negative response (blue color) first, followed by a positive (red) response, and then blue again, as shown in figures 5 through 8, and vice versa for the metal corn models. For example, for the large natural corn seed (fig. 6), the first blue color response can be seen at the top and the second blue response at the bottom, with red in between. These color contrasts were more apparent for the large natural corn seed model with an increase in soil VMC.

In practice, the response amplitude needed to detect the presence of a target depends on the contrast between the electrical properties of the target and of the surrounding medium. The results of the simulation models in this study indicate that natural corn seeds could be detected by GPR waves, under certain conditions.

Simulation Model Verification

The gprMax simulation models developed in this study correspond with other work on the detection of dielectric and conductive targets. Twizere (2011) showed that an increase in soil clay content led to an increase in dielectric properties, particularly the effective dielectric constant, of the soil model. According to his model evaluation, the wave velocity decreased rapidly due to the high dielectric constant and absorption, and the reflection of the waves increased at high soil density. Thus, a limited amount of GPR energy can penetrate the surface, with higher time delays and rapid attenuation. This phenomenon corresponds to the findings of our study, in which no corn seed response amplitudes were observed in the soil with high clay content with both low and high VMC.

Miller et al. (2002) showed that moist soils and clay soils markedly attenuated GPR waves. In our study, GPR waves

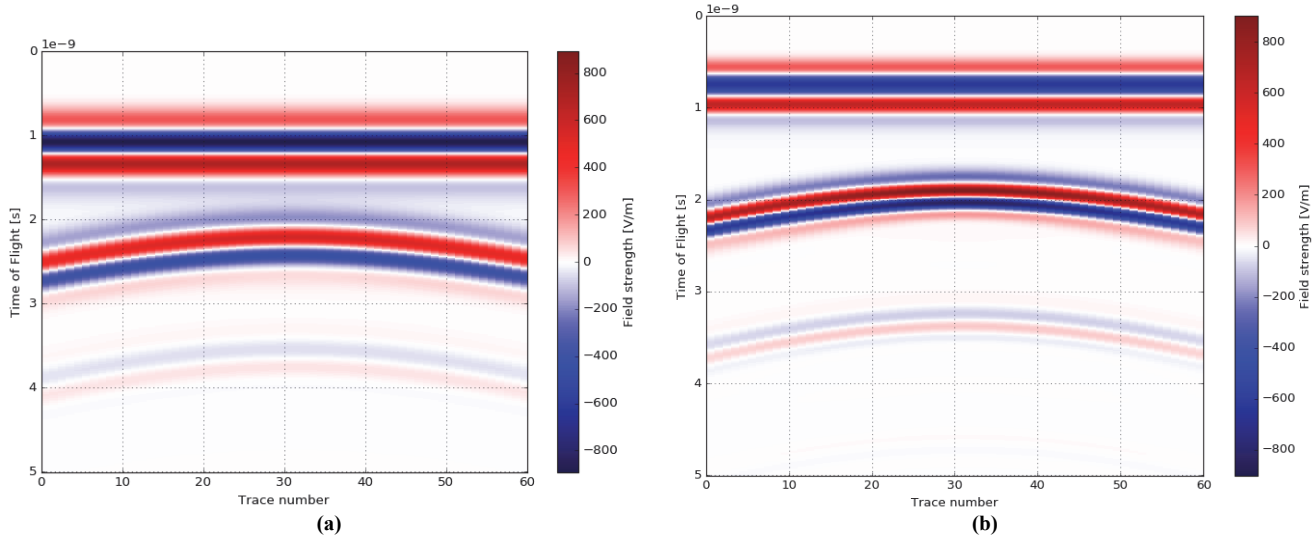

Figure 8. Response of large metal corn seed model (0.024 m radius) in sandy loam at 15% VMC and soil bulk density of 1.42 g cm^{-3}: (a) B-scan at center frequency of 1.6 GHz, and (b) B-scan at center frequency of 2.6 GHz.

entering the soil surface decreased proportionally with an increase in VMC. Our simulation results indicated that corn seed models provided better response amplitudes as the VMC increased from 2.5% to 40%, which coincides with the results of Miller et al. (2002). Their results showed that nonmetallic landmines with dielectric constants of 3.2 were more detectable at higher soil moisture rather than at lower moisture. At lower VMC, there was not enough contrast between the soil and the nonmetallic landmine to provide a substantial response, similar to our study. The metal corn seed models were highly responsive to GPR waves in all soil conditions. However, at higher VMC, the response amplitudes tended to decrease.

GPR has been considered by agricultural researchers as a method to improve data collection for precision agriculture applications, such as measuring soil moisture, locating drainage pipes and hardpans, and studying root morphology and biomass. Butnor et al. (2001) investigated tree root biomass in soil with high clay and VMC. Attenuation was rapid, and the assessed depth was severely restricted (Butnor et al., 2001). Butnor et al. (2001) used two antenna center frequencies (400 MHz and 1.5 GHz) and reported that 1.5 GHz provided higher resolution and distinguished more roots in the upper soil profile compared to 400 MHz. In our simulations, the dielectric corn seed provided higher response amplitudes at 2.6 GHz compared to 1.6 GHz. Butnor et al. (2001) also demonstrated that root size had a profound effect on response amplitude: the larger the target, the higher the response amplitude. They also indicated that the root moisture content had a significant impact on the detectability of roots.

Our gprMax simulation results align with the results reported by Butnor et al. (2001). A positive implication for GPR detection of *in situ* corn seeds is that seeds are live grains and have a certain moisture content. In our simulations, the corn seed dielectric constant was estimated using a moisture content of 11.00%. The estimated dielectric constant created a substantial dielectric contrast between the seed model and the surrounding soil model, which led to the proportional GPR wave response amplitudes presented in this article. For the natural corn seed model, the dielectric contrast resulted in increasing response amplitudes that were proportional to the increase in soil VMC for the different soil types.

Experimental Verification

The simulation results indicated that corn seeds could be detected in certain soil conditions, with strong response amplitudes (tables 4 through 6) or hyperbolic responses (figs. 5 through 8). Based on the simulation results, we opted to use soils with low electrical conductivity (non-saline), low clay content, and low bulk density for possible mapping of corn seeds. In sandy loam soil using a 2.6 GHz antenna, the response amplitudes (table 6) were much improved compared to the 1.6 GHz antenna results (table 4). Because the soil models were homogeneous, real soils were processed (crushed and sieved to remove clods and other sediments) and prepared accordingly.

Laboratory experiments were performed under controlled conditions in soil bins using a 2.6 GHz GPR antenna. A non-saline sandy loam soil with 67% sand, 25% silt, 8% clay, and a measured density of 1.41 g cm^{-3} was used for the validation. Three soil moisture contents, classified as dry (2.95% average), low (11.34% average), and medium (16.67% average), were assessed. The measured VMCs of 2.95%, 11.34%, and 16.67% corresponded to the simulation VMCs of 2.50% to approximately 15.00%. The corn seeds were variety P0339AMXT with Precision Design Round size (Pioneer Hybrids, Johnson, Iowa) with a measured moisture content of 10.05% (corresponding to the 11% corn moisture content used in the simulations). A low soil VMC of 11.34% and corn seed moisture content of 10.05% created an environment in which GPR might not detect the corn seeds because the corn and soil moisture contents were similar. The corn seeds were buried at three depths (0.0381, 0.0635, and 0.0889 m) and two seed spacings (0.1524 and 0.254 m). Five replicates were collected per soil moisture level. Data were processed using the matGPR package to enhance readability and interpretation (Tzanis, 2013, 2015). The acquired data

were first filtered to suppress horizontal bands, ringing noise, reverberations, and clutter in the B-scans. In some cases, filtering suppressed pixels with important target information, making detection of the target more difficult. Fast discrete curvelet transform (FDCT) was then used to clarify edges within the images, followed by an edge-detection algorithm to enhance the images (Tzanis, 2013, 2015). The algorithm parameters used in the filtering were dependent on each B-scan.

Experimental Results

The GPR data collected in the verification experiment showed mixed success. Figures 9 and 10 show raw B-scans with partial detection of corn seeds and processed B-scans with enhanced edges and reduced clutter or noise.

The B-scan in figure 9a was collected in dry sandy loam in which not all buried corn seeds were detected. Shallower seeds had the highest probability of being detected. The deeper the corn seeds were buried, the harder they were to detect. Moreover, in some of the replicated B-scans, no traceable responses were visible in the raw or processed image. In general, drier soils presented greater probability that corn seeds could be detected. Even though the soils were dry, it is evident from figure 9a that seed responses were evanescent, quickly fading as the GPR wave traversed deeper depths, and the targets exhibited faint hyperbolic responses. However, in our simulation results, no response amplitude was registered in dry soils. GPR waves are sensitive to moisture, and the sandy loam soil and field corn had average moisture contents of 2.95% and 10%, respectively. The moisture difference (7.1%) between the two materials may have contributed to the detectability of corn seeds in the laboratory tests, which was not like the simulation results. In the simulation, the dielectric contrast between the soil model (ε = 3.41 or 4.25 at 2.5% or 5% VMC) and corn model (ε = 3.9 at 11% moisture) was approximately 0.35 or 0.49, which did not create a strong dielectric contrast.

The simulation results indicated that corn seeds could be detected in medium moisture conditions due to the high dielectric contrast. However, in the experimental results, low dielectric contrast was observed between the surrounding soil and the corn seeds in moist sandy loam (fig. 10a). If there was any dielectric contrast between the two materials, it was probably masked by other factors within the soil ma-

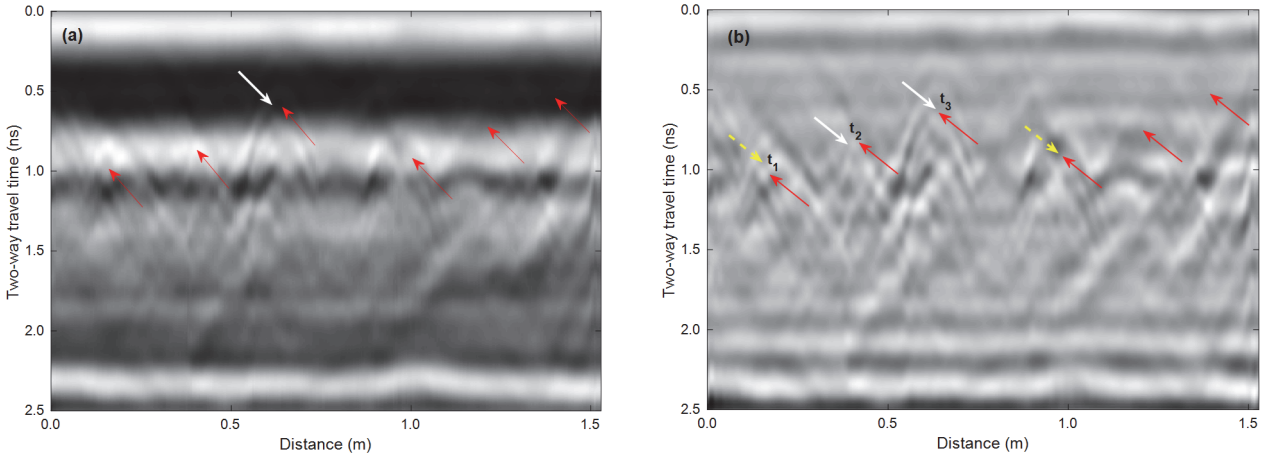

Figure 9. (a) Raw and (b) processed GPR data collected from dry sandy loam soil. Red arrows indicate nominal corn seed positions, yellow arrows indicate responses that could be corn seeds or clutter, and white arrows indicate approximate corn responses (t_1, t_2, and t_3 represent the time of flight to the corn seeds, which corresponds to the nominal depth).

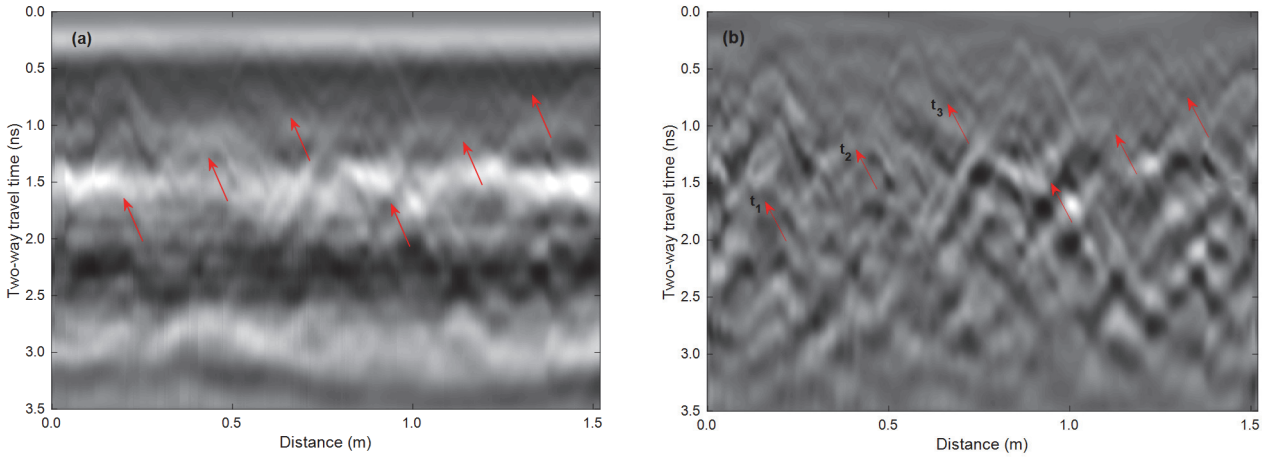

Figure 10. (a) Raw and (b) processed GPR data collected from moist sandy loam soil. Red arrows indicate corn seed positions.

Table 7. Experimental results obtained from different VMC values and soil bulk density of 1.41 g cm^{-3} in sandy loam using an antenna frequency of 2.6 GHz and field corn variety P0339AMXT PDR.

Volumetric Moisture Content (VMC, %)		Peak Response Amplitude (V m^{-1})	Nominal Time Corresponding to Corn Seed Depth	
			Time Point	Time of Flight
Dry	2.95	1076	t_1	0.92 ns
	2.93	1064	t_2	0.68 ns
	2.33	1815	t_3	0.54 ns
Low	10.85	1198	t_1	1.43 ns
	10.46	619	t_2	1.08 ns
	11.34	814	t_3	0.75 ns
Medium	15.80	248	t_1	1.62 ns
	15.03	397	t_2	1.12 ns
	17.07	602	t_3	0.87 ns

trix, such as the attenuation of waves, slower wave velocity due to higher moisture, and irregular reflections due to clutter. The processed B-scan (fig. 10b) shows multiple hyperbolic responses, which suggests that corn seed responses could be among the several responses. Therefore, based on the raw and processed B-scans in figure 10, we indicated locations where corn seeds could reside. Multiple reflections, where corn seeds were thought to be, made it difficult to discern which responses were from corn seeds. This phenomenon was observed across the replicates collected at low and medium soil VMC.

The extracted time of flight (TOF) and response amplitude for the dry, low, and medium VMC soils are shown in table 7. The TOF and response amplitude data were extracted from the processed B-scans (figs. 9b and 10b) using a FORTRAN algorithm. In the algorithm, the apex of the hyperbolic response is identified in the B-scan by specifying a window in which the algorithm resolves the two parameters automatically. Features were defined in dry soils (less interference), which made it easier to specify the window in which to extract the information compared to wetter soils due to the high level of clutter. The extracted TOFs were adjusted to remove the coupling time at the soil-air interface (time zero-correction). The TOFs can be used to estimate nominal corn seed depths. Table 7 shows that the response amplitudes in dry VMC soils were high compared to the low and medium VMC soils.

An opposite trend in peak response amplitude was observed between the simulation results (table 6) and the experimental results (table 7). The time of flight followed the same trend in the verification experiment as in the simulation. At low VMC, the detection time was quicker; conversely, at high VMC, detection was slower.

CONCLUSION

Using ground-penetrating radar (GPR) for seed depth detection is highly dependent on the soil physical properties and on the contrast between the dielectric properties of the seed and the surrounding soil matrix. Two-dimensional gprMax simulation models were developed for preliminary evaluation of the potential of using GPR for seed depth detection. Laboratory experiments were conducted to validate the trends exhibited in the simulation results. The overall conclusions from this study include:

- The simulation results predicted that GPR could be used to locate natural corn seed models in certain soil conditions, including low clay content and low soil bulk density. There was substantial attenuation in soils with high clay content and high bulk density, which made successful seed detection unlikely.
- A higher frequency (2.6 GHz) was determined to have better probability of detecting small (standard size) corn seeds.
- The simulation results predicted that response amplitudes were better at 40%, 25%, and 15% soil VMC and low to negligible at 5%, and 2.5% soil VMC. Dielectric contrast between the seed and the soil was necessary for detection.
- Laboratory experiments showed that 2.6 GHz could detect shallow corn seeds in dry soil conditions; however, as seed depth increased, GPR wave strength rapidly decayed, leading to no detection.
- In the laboratory tests, corn seed detection became increasingly difficult at higher soil moisture contents. At higher moisture contents, clutter due to constructive and destructive interference between multiple overlapping hyperbolic responses resulted in greater clutter in the B-scans. This was not consistent with the simulation results.
- The results from the simulation model aligned with work performed by several researchers in locating buried metal and dielectric (roots) targets in different soil conditions.

The simulation and experimental results indicated that GPR has potential to locate corn seeds in sand, loam, and low clay content soils (unless the soil bulk density is high) at specific soil moisture contents. The overall conclusion is that detecting buried corn seeds in soils may be possible using GPR, but the method requires additional study to determine if robust and reliable detection of buried corn seeds is possible under all necessary field conditions.

REFERENCES

Allred, B. J., Daniels, J. J., Fausey, N. R., Chen, C., Peters Jr., L., & Youn, H. (2005). Important considerations for locating buried agricultural drainage pipe using ground-penetrating radar. *Appl. Eng. Agric., 21*(1), 71-87. https://doi.org/10.13031/2013.17915

Allred, B. J., Fausey, N. R., Peters Jr., L., Chen, C., Daniels, J. J., & Youn, H. (2004). Detection of buried agricultural drainage pipe with geophysical methods. *Appl. Eng. Agric., 20*(3), 307-318. https://doi.org/10.13031/2013.16067

Allred, B., Daniels, J. J., & Ehsani, M. R. (2008). *Handbook of agricultural geophysics.* Boca Raton, FL: CRC Press. https://doi.org/10.1201/9781420019353

Annan, A. P. (2009). Electromagnetic principles of ground-penetrating radar. In *Ground-penetrating radar: Theory and applications* (pp. 1-40). Amsterdam, The Netherlands: Elsevier. https://doi.org/10.1016/B978-0-444-53348-7.00016-8

Beck's Hybrids. (2014). *Practical farm research (PFR).* Atlanta, IN: Beck's Hybrids. Retrieved from https://www.beckshybrids.com/Portals/0/SiteContent/Literature/2015%20Literature/2014-Practical-Farm-Research-PFR-Book.pdf

Brisco, B., Pultz, T. J., Brown, R. J., Topp, G. C., Hares, M. A., & Zebchuk, W. D. (1992). Soil moisture measurement using

portable dielectric probes and time domain reflectometry. *Water Resour. Res., 28*(5), 1339-1346. https://doi.org/10.1029/92WR00057

Butnor, J. R., Doolittle, J. A., Kress, L., Cohen, S., & Johnsen, K. H. (2001). Use of ground-penetrating radar to study tree roots in the southeastern United States. *Tree Physiol., 21*(17), 1269-1278. https://doi.org/10.1093/treephys/21.17.1269

Chaudhari, H. C. (2015). Dielectric study of soils with varied organic matter at microwave frequency. *Intl. J. Chem. Phys. Sci., 4*(3), 45-53.

Chen, Q., Jiuli, L., Zhihua, T., Jiangyuan, Z., & Li, Y. (2014). Study on the relationship between soil moisture and its dielectric constant obtained by space-borne microwave radiometers and scatterometers. *IOP Conf. Series: Earth Environ. Sci., 17*(1), 012143. Retrieved from http://stacks.iop.org/1755-1315/17/i=1/a=012143

Datta, A. K. (2001). *Handbook of microwave technology for food application.* Boca Raton, FL: CRC Press. https://doi.org/10.1201/9781482270778

Doerge, T., Jeschke, M., & Carter, P. (2015). Planting outcome effects on corn yield. *Crop Insights, 25*(1), 1-7.

ECT. (2013). Conductivity of metals sorted by resistivity. Virginia Beach, VA: Eddy Current Technology Inc. Retrieved from http://eddy-current.com/conductivity-of-metals-sorted-by-resistivity/

Elmore, R., Al-Kais, M., & Hanna, M. (2014). Corn seeding depth: Back to the basics. *Agronomy News, 5*(1), 1-3. Cambridge, MD: University of Maryland Extension. Retrieved from http://extension.umd.edu/sites/extension.umd.edu/files/_docs/newsletters/Agronomy%20News%20May%201%202014.pdf

Flores, A. N., Ivanov, V. Y., Entekhabi, D., & Bras, R. L. (2009). Impact of hillslope-scale organization of topography, soil moisture, soil temperature, and vegetation on modeling surface microwave radiation emission. *IEEE Trans. Geosci. Remote Sensing, 47*(8), 2557-2571. https://doi.org/10.1109/TGRS.2009.2014743

Hajnsek, I., & Papathanassiou, K. (2005). Rough surface scattering models. Paris, France: European Space Agency. Retrieved from https://earth.esa.int/documents/653194/656796/Rough_Surface_Scattering_Models.pdf

Hendrickx, J. M. H., Van Dam, R. L., Borchers, B., Curtis, J. O., Lensen, H. A., & Harmon, R. S. (2003). Worldwide distribution of soil dielectric and thermal properties. *Proc. SPIE 5089*, 1158-1168. Bellingham, WA: SPIE. https://doi.org/10.1117/12.487116

Hillel, D. (2003). *Introduction to environmental soil physics.* Amsterdam, The Netherlands: Elsevier.

Howlader, M. O. F., & Sattar, T. P. (2015). FDTD based numerical framework for ground-penetrating radar simulation. *Prog. Electromag. Res. M, 44*, 127-138. https://doi.org/10.2528/PIERM15090304

Hussen, S., Alemu, B., & Ahmed, F. (2013). Effect of planting depth on growth performance of maize (*Zea mays*) at the experimental site of Wollo University, Dessie, Ethopia. *Intl. J. Sci. Basic Appl. Res. (IJSBAR), 8*(1), 10-15.

Jol, H. M. (2009). *Ground-penetrating radar: Theory and applications.* Amsterdam, The Netherlands: Elsevier.

Ketata, M., Dhieb, M., Chaoui, M., Lahiani, M., & Ghariani, H. (2010). Electric field attenuation of an ultra wide band wave (UWB) during propagation in the human body. *Intl. J. Sci. Tech. Auto. Control Comput. Eng., 4*(1), 1188-1197.

Kunz, K. S., & Luebbers, R. J. (1993). *The finite difference time domain method for electromagnetics.* Boca Raton, FL: CRC Press.

Mészáros, P. (2007). Relationships between electrical parameters and physical properties of cereal grains, oilseeds, and apples. Budapest, Hungary: Corvinus University of Budapest. Retrieved from http://phd.lib.uni-corvinus.hu/31/1/peter_meszaros.pdf

Miller, T. W., Borchers, B., Hendrickx, J. M. H., Hong, S.-H., Lensen, H. A., Schwering, P. B. W., & Rhebergen, J. B. (2002). Effect of soil moisture on landmine detection using ground-penetrating radar. *Proc. SPIE 4742.* Bellingham, WA: SPIE. https://doi.org/10.1117/12.479124

Miller, T. W., Hendrickx, J. M. H., & Borchers, B. (2004). Radar detection of buried landmines in field soils. *Vadose Zone J., 3*(4), 1116-1127. https://doi.org/10.2136/vzj2004.1116

Mur, G. (1981). Absorbing boundary conditions for the finite-difference approximation of the time-domain electromagnetic-field equations. *IEEE Trans. Electromagnetic Compatibility, EMC-23*(4), 377-382. https://doi.org/10.1109/TEMC.1981.303970

Mur, G. (1998). Total-field absorbing boundary conditions for the time-domain electromagnetic field equations. *IEEE Trans. Electromag. Compatibility, 40*(2), 100-102. https://doi.org/10.1109/15.673614

Neal, A. (2004). Ground-penetrating radar and its use in sedimentology: Principles, problems, and progress. *Earth Sci. Rev., 66*(3-4), 261-330. http://dx.doi.org/10.1016/j.earscirev.2004.01.004

Nelson, S. O. (1987). Models for the dielectric constants of cereal grains and soybeans. *J. Microwave Power Electromag. Energy, 22*(1), 35-39. https://doi.org/10.1080/08327823.1987.11688004

Nelson, S. O. (2005). Dielectric properties measurement for agricultural applications. ASAE Paper No. 053134. St. Joseph, MI: ASAE. https://doi.org/10.13031/2013.19107

Nelson, S. O. (2015). *Dielectric properties of agricultural materials and their applications.* Amsterdam, The Netherlands: Elsevier.

Nelson, S. O., & Datta, A. K. (2001). Dielectric properties of food materials and electric field interactions. In *Food science and technology* (pp. 69-114). Boca Raton, FL: CRC Press.

Nielsen, R. (2001). Stand establishment variability in corn. West Lafayette, IN: Purdue University, Department of Agronomy. Retrieved from https://www.agry.purdue.edu/ext/pubs/AGRY-91-01_v5.pdf

Norimoto, M. (1976). Dielectric properties of wood. Kyoto, Japan: Kyoto University. Retrieved from https://core.ac.uk/download/pdf/39187623.pdf

NSSC. (2011). *Soil survey laboratory information manual*. Lincoln, NE: USDA-NRCS National Soil Survey Center. Retrieved from https://www.nrcs.usda.gov/Internet/FSE_DOCUMENTS/nrcs142p2_052226.pdf

Odhiambo, L. O., Freeland, R. S., Yoder, R. E., & Wesley Hines, J. (2002). Application of fuzzy-neural network in classification of soils using ground-penetrating radar imagery. ASAE Paper No. 023097. St. Joseph, MI: ASAE. https://doi.org/10.13031/2013.11691

Orfanidis, S. J. (2002). *Electromagnetic waves and antennas.* New Brunswick, NJ: Rutgers University.

Peplinski, N. R., Ulaby, F. T., & Dobson, M. C. (1995). Dielectric properties of soils in the 0.3 to 1.3 GHz range. *IEEE Trans. Geosci. Remote Sensing, 33*(3), 803-807. https://doi.org/10.1109/36.387598

René-Laforest, F., Adamchuk, V. I., Mastorakos, M. A., Dhawale, N. M., & Su, Y. (2014). Variable-depth planting of corn. ASABE Paper No. 141912822. St. Joseph, MI: ASABE. https://doi.org/10.13031/aim.20141912822

Sadiku, M. N. (2010). *Elements of electromagnetics* (5th ed.). Cary, NC: Oxford University Press.

Sato, M. (2009). Principles of mine detection by ground-penetrating radar. In *Anti-personnel landmine detection for humanitarian demining* (pp. 19-26). Berlin, Germany: Springer. https://doi.org/10.1007/978-1-84882-346-4_2

Sayre, J. D. (1940). Storage tests with seed corn. *Farm Home Res., 32*(247), 149-154.

Schneider, J. B. (2010). Understanding the finite-difference time-domain method. Pullman, WA: Washington State University, School of Electrical Engineering and Computer Science. Retrieved from https://www.eecs.wsu.edu/~schneidj/ufdtd/ufdtd.pdf

Topp, G. C., Davis, J. L., & Annan, A. P. (1980). Electromagnetic determination of soil water content: Measurements in coaxial transmission lines. *Water Resour. Res., 16*(3), 574-582. https://doi.org/10.1029/WR016i003p00574

Trabelsi, S., & Nelson, S. O. (2003). Free-space measurement of dielectric properties of cereal grain and oilseed at microwave frequencies. *Meas. Sci. Tech., 14*(5), 589. https://doi.org/10.1088/0957-0233/14/5/308

Twizere, C. (2011). Use of GPR techniques for landmines detection and road monitoring. PhD diss. Rome, Italy: Roma Tre University. Retrieved from http://dspace-roma3.caspur.it/bitstream/2307/4564/1/FinalThesisTwizere.pdf

Tzanis, A. (2013). Detection and extraction of orientation-and-scale-dependent information from two-dimensional GPR data with tuneable directional wavelet filters. *J. Appl. Geophys., 89*, 48-67. https://doi.org/10.1016/j.jappgeo.2012.11.007

Tzanis, A. (2015). The curvelet transform in the analysis of 2-D GPR data: Signal enhancement and extraction of orientation-and-scale-dependent information. *J. Appl. Geophys., 115*, 145-170. https://doi.org/10.1016/j.jappgeo.2015.02.015

Warnick, K. F. (2011). *Numerical methods for engineering: An introduction using MATLAB and computational electromagnetics examples.* Stevenage, UK: SciTech Publishing. https://doi.org/10.1049/SBEW049E

Warren, C., Giannopoulos, A., & Giannakis, I. (2016). gprMax: Open-source software to simulate electromagnetic wave propagation for ground-penetrating radar. *Comput. Phys. Comm., 209*, 163-170. https://doi.org/10.1016/j.cpc.2016.08.020

Weiler, K. W., Steenhuis, T. S., Boll, J., & Kung, K.-J. S. (1998). Comparison of ground-penetrating radar and time-domain reflectometry as soil water sensors. *SSSA J., 62*(5). https://doi.org/10.2136/sssaj1998.03615995006200050013x

Yee, K. S. (1966). Numerical solution of initial boundary value problems involving Maxwell's equations in isotropic media. *IEEE Trans. Antennas Prop., 14*(3), 302-307. https://doi.org/10.1109/TAP.1966.1138693

Yoder, R. E., Freeland, R. S., Ammons, J. T., & Leonard, L. L. (2001). Mapping agricultural fields with GPR and EMI to identify offsite movement of agrochemicals. *J. Appl. Geophys., 47*(3), 251-259. https://doi.org/10.1016/S0926-9851(01)00069-6

Zhang, R., Zhang, D., Yang, L., & Yan, B. (2015). Optimal design and simulation analysis on a sowing depth control unit for corn precision planter. ASABE Paper No. 152189688. St. Joseph, MI: ASABE. https://doi.org/10.13031/aim.20152189688